UC Irvine
UC Irvine Electronic Theses and Dissertations

Title
Controlled synthesis of nanoparticles using the alternating current method

Permalink
https://escholarship.org/uc/item/4sj1r9tq

Author
pan, dingjie

Publication Date
2020

Peer reviewed|Thesis/dissertation

eScholarship.org Powered by the California Digital Library
University of California

UNIVERSITY OF CALIFORNIA,
IRVINE

Controlled synthesis of nanoparticles using the alternating current method

Thesis

Submitted in partial satisfaction of the requirements for the degree of

MASTER OF SCIENCE

in Material Science and Engineering

by

Dingjie Pan

Dissertation Committee:

Professor Iryna Zenyuk, Chair

Professor Plamen Atanassov

Professor Erdem Sasmaz

2020

© 2020 Dingjie Pan

DEDICATION

To

my parents

my girlfriend Weishi Liang

in recognition of their support and help

TABLE OF CONTENTS

LIST OF FIGURES

LIST OF TABLES

ACKNOWLEDGMENTS

I would like to sincerely appreciate my thesis advisor and committee chair, Professor Iryna Zenyuk, who offer me an opportunity to explore in the field of fuel cell and platinum nanocatalyst in her group. Without the encouragement and inspiration from Iryna, I will not make progress in research. I would also like to appreciate to Professor Plamen Atanassov and Professor Erdem Sasmaz for becoming my thesis committee and providing insightful suggestions on my thesis research.

I would like to deeply gratitude to the IRD fuel cell for funding my research.

During the two-year study at the Iryna group, I receive helpful advice from my colleagues. It is my great honor to cooperate with Dr. Andrea Perego and Dr. Tristan Francois Asset. Thanks to Yongzhen Qi for leading me patiently when I was a beginner. Thanks to Arezoo Avid for kindly guiding me in RDE research. Thanks to the National Fuel Cell Research Center for providing me a great experiment environment.

ABSTRACT OF THE THESIS

Controlled synthesis of nanoparticles using the alternating current method

By

Dingjie Pan

Master of Science in Material Science and Engineering

University of California, Irvine, 2020

Fuel cells can potentially become a practical solution for solving the emerging energy crisis. Platinum nanoparticles are used as electrocatalyst for oxygen reduction reaction. Many synthesis methods exist that produce platinum nanoparticles supported by carbon support. The goal for synthesis is to increase its performance and reduce its loading. In this paper, we successfully synthesized Pt nanoparticles within 2.09 ± 0.76 nm range with the alternating current method. With this one-step, top-down method, Pt nanoparticles were produced by simply applying the square wave potential to the Pt wire without adding any additional chemicals. Besides, the rotating disk electrode (RDE) measurements suggest this method has a possibility to increase the performance of the Pt nano catalyst.

Moreover, we explored the mechanism of the generation of nanoparticles and proposed the critical potential range for this method. And we first reported the Pt formation in neutral and acid electrolyte.

Chapter 1 Introduction

1.1 A brief overview of the energy revolution

Energy is one of the essential elements to ensure human civilization. Throughout human history, the three transformations in energy development took place. These transformation were: from wood to coal, then to oil and gas, and now and in the future renewable energy will be the next transformation. Before the 18th century, humans were limited to the direct use of natural energy sources such as wind, water, animal power, and wood. The reformation of the steam engine by James Watt in 1769 accelerated the development of the coal industry and coal surpassed wood as the largest share in the primary energy mix in the 1780s. In 1885, the invention of the internal combustion engine by Gottlieb Wilhelm Daimler motivated the requirement of oil and gas. In 1979, the proportion of the sum of oil and gas in the world's energy consumption structure was 72 % and replaced coal to complete the second conversion of energy. (1) However, the reserve of oil on the earth is limited, and the increased demount of oil consumption has caused the shortage of energy supply and the rise of extreme weather events. The increased ocean acidity and the shrinking of the glacial landmass were due to global warming. (2) In 2015, 196 states reached the Paris agreement to control the increase of global average temperature within 2 ℃ above the pre-industrial level. (3,4) The third transformation of energy from fossil fuel to non-fossil fuel new energy is imperative. And the development of the clean energy industry is not only for meeting the target of temperature rise but also marketing driven. (5,6) And the zero-emission fuel cell vehicles with high efficiency and fast charging is the key to reducing the emission from the transportation sector. (7,8)

1.2 The introduction of polymer electrolyte fuel cells (PEFCs)

Fuel cells, as electrochemical devices, convert the chemical energy from fuels into electrical energy directly, promise high efficiency of power generation, and negligible environmental impact (9). Tracing back to 1839, the publication, which reported a current produced from the combination of hydrogen and oxygen by Christian Friederich Schönbein (10) is the origin of the fuel cell. (11) Figure 1.1 is a schematic of the basic fuel cell operation.

Typically, fuel and oxidant (oxygen from the air, generally) are fed continuously and separately to the anode and cathode, respectively. The triple-phase boundary (TPB), the interface between the gas electrode and electrolyte phases, is the place for the occurrence of electrochemical reactions (on a molecular scale). Pure H_2 reaches to the TPB on the anode side through the gas diffusion layer (GDL) and the hydrogen oxidation reaction (HOR) is accelerated by the anode catalyst and the remaining fuel and exhaust are expelled from the unit cell. The proton (H^+) transfers to the cathode through the ion-conducting electrolyte (proton exchange membrane) by the ionic potential gradient, as the driving force while electrons generated by the HOR travel through the external circuit to the cathode. Once the proton and oxygen reache the surface of the cathode, the oxygen reduction reaction (ORR) takes place on the TPB at the cathode. The produced water as the byproduct is removed by the remaining air in the gas flow-field (9).

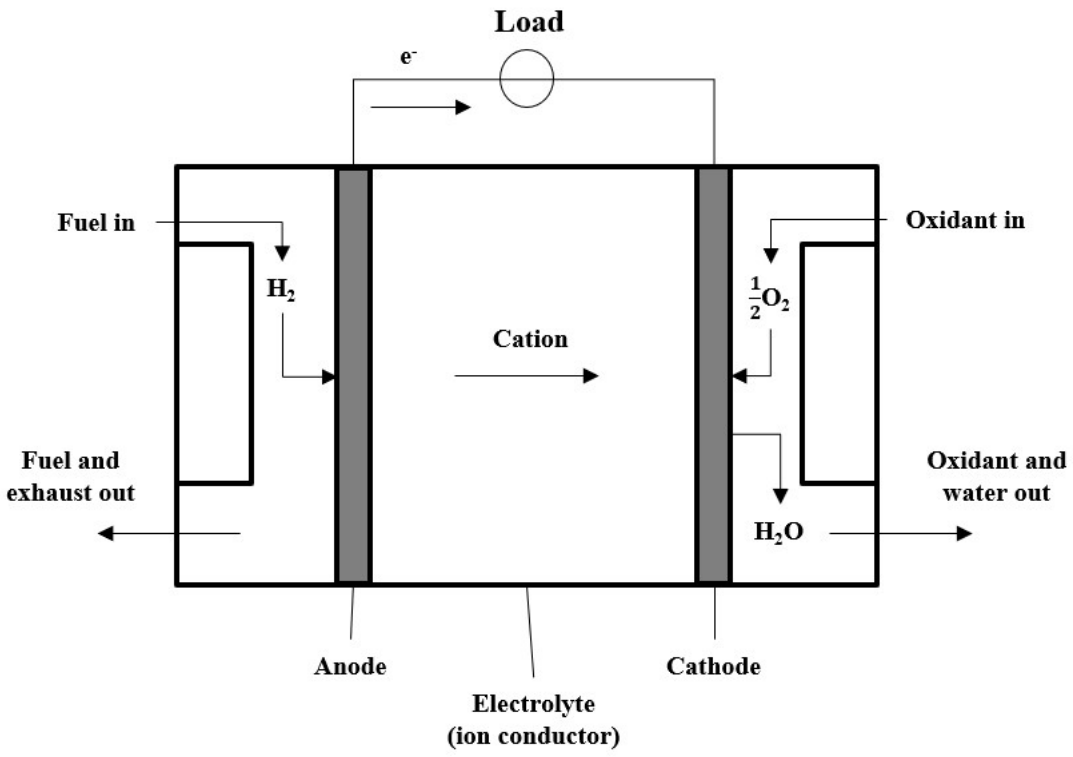

Figure 1.1 The design of fuel cell unit cell, where transport processes are shown too.

HOR at the anode side: $H_2 \rightarrow 2H^+ + 2e^-$ 0 V

ORR at the cathode side: $\frac{1}{2}O_2 + 2H^+ + 2e^- \rightarrow H_2O$ 1.23 V

Depending upon chemical potential difference rather than the thermodynamic driving force, fuel cells produce electricity directly using electrochemistry and avoid multiple intermediate conversion steps of producing heat and mechanical work, which are inevitable for conventional heat engines (9). Thus, not limited by the Carnot efficiency (12), PEFCs operate at 50 – 80 °C, and have 45 – 60 % fuel efficiency and 40 – 70 % voltage efficiency (13,14). Compared with batteries, fuel cells have high energy and fast refueling speed. Additionally, since combustion is avoided, fuel cells produce power with zero to ultra-low pollutant emission and very low noise levels (9). However, the cost limits the popularization of fuel cells as platinum is one of the

costly components in PEFCs. To accelerate the HOR and ORR at low temperatures (50 – 80 ℃), the catalyst layers consisting of 2 – 5 nm platinum nanoparticles supported on 20 – 30 nm primary carbon particles bound with 2 – 70 nm thin-film ionomer coatings are critical porous layers in the PEFCs (8,15–17).

In this thesis, we focus on reducing the cost by generating the Pt nanoparticles with high purity, uniform size and better performance to reduce the amount of Pt in PEFCs and to enable cleaner manufacturing method.

1.3 The alternating current method of synthesizing Pt nanoparticles catalyst layers

For commercial fuel cell vehicle, the catalyst layers of cathode and anode in PEFCs are composed of Pt-based nanostructures supported on high surface area carbon. (18) To reduce the amount of costly platinum catalyst, producing small size Pt nanoparticles to maximize the surface-to-volume ratio is necessary. In general, for producing the Pt nanoparticles with size-controlled and desirable characteristics for various applications, three groups of synthesis methods (physical, chemical, and biological) are adopted. Laser ablation, arc discharge, vapor deposition, melt mixing, ball milling, sputter deposition, and flame pyrolysis are available for physical methods. Though physical methods have various advantages including high speed, high purity, uniform size and shape, and no toxic chemicals, the high cost, lower thermal stability, high requirement of energy, temperature, and pressure limit the widely use of physical methods. For cost-effective chemical methods, metal monomers are reduced from cation in the solution, and extra chemicals as stabilizers are added inevitably to keep the constant size. The use of toxic chemicals and organic solvents causes low purity and the environmental damage. Biological methods with the aim of being environmentally friendly are difficult to use to control the shape,

size, aggregation, and the growth of crystals. Besides, the purification process of removing the bacteria is time-consuming. (19)

In this paper, we introduce a top-down synthesis method via the electrochemical breakdown of the macroscopic metal wire by apply alternating current. For synthesizing platinum nanoparticles, a square wave potential is applied to two Pt wires, which are immersed in alkaline solution. Pt nanoparticles are generated from wires immediately along with the gas bubbles. According to the Pourbiax diagram of platinum (20) in Figure 1.2 (cited from the published paper), above the standard reduction potential (21), platinum dissolves and forms platinum ions.

The standard reduction potential of Pt vs RHE:

$$Pt^{2+} + 2e^{-} \rightarrow Pt \qquad 1.2\,V$$

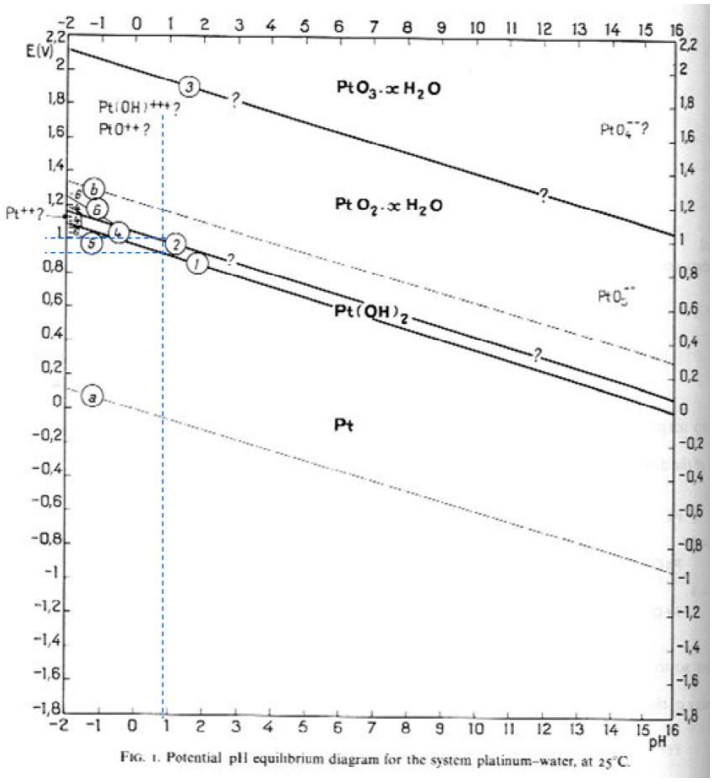

FIG. 1. Potential pH equilibrium diagram for the system platinum–water, at 25°C.

Figure 1.2 The Pourbiax diagram of platinum, reproduced from Ref. (20)

With better size and shape control and no additional chemicals, this single-step method of nanoparticles synthesis was first published in 1898 then was further explored by Kabanov in 1979 for the preparation of intermetallic compounds and in this century, great progress was made by several groups and the method was named as cathodic corrosion. (22–47) Thanks to these studies, the knowledge of size and shape control and platinum performance was well correlated. Whereas the understanding of alternating current electrochemistry is insufficient and lack of experiments focusing on the mechanisms for the synthesis of nanoparticles with the AC method. Current explanations of the nanoparticle generation are (1) cathodic corrosion; (2) micro explosion and (3) cation effect.

The mechanism of the cathodic corrosion hypothesis is shown in Figure 1.3. The alternating current is superimposed by positive charge and negative charge for each cycle, the phenomenon transforms into two direct current conditions. Under a high positive voltage, electrons are extracted, and an oxidation reaction happens. The Pt wire and oxygen anions in the solution are oxidized to PtO and O_2, respectively. While under the negatively applied potential, electrons are pumped into the wire, forcing the PtO and hydrogen cations to reduce to Pt and H_2, respectively. The continuous formation of gas brings the newly synthesized platinum nanoparticles, which are not well attach to the wire, into the solution and produce Pt nanoparticles (48). However, the generation of alloy nanoparticles reported with this method (22) contradicts the corrosion theory, since the different standard potentials of two metals should result in dissolution of one metal and not the other. However, previous study showed that with the AC method we can generate alloy metal.

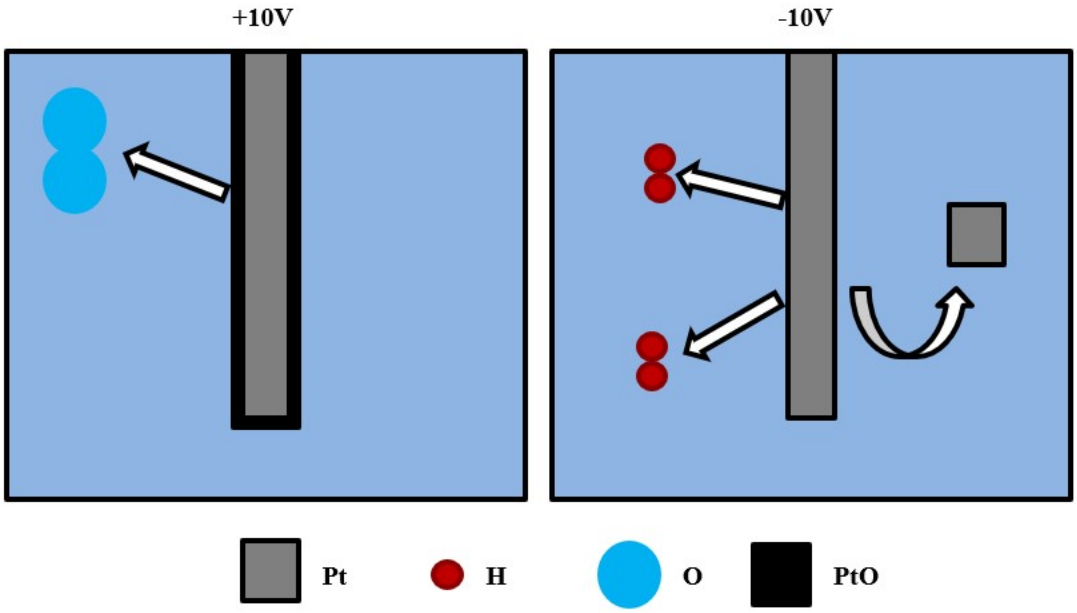

Figure 1.3 The mechanism of cathodic corrosion hypothesis , where metal wire is shown during + 10 V (left) and – 10 V (right), where oxygen evolution reaction occurs at +10 V and hydrogen evolution happens at -10 V. Pt particles are produced during – 10 V.

Figure 1.4 shows the mechanism of the micro explosion (49) theory. The AC potentials applied to the Pt wire are above the dissociation potential of both hydrogen and water (1.23 V) (21) leading to the formation of H_2 and O_2 on the same Pt wire in the negative and positive voltage sweep, respectively. The mixture of H_2 and O_2 in the outer layer causes the micro explosion in the solution and Pt nanoparticles are mechanically removed from the wire due to the stress induced by this micro explosion. The SEM image (43,49) of the rough surface of Pt wire after experiment supports this theory.

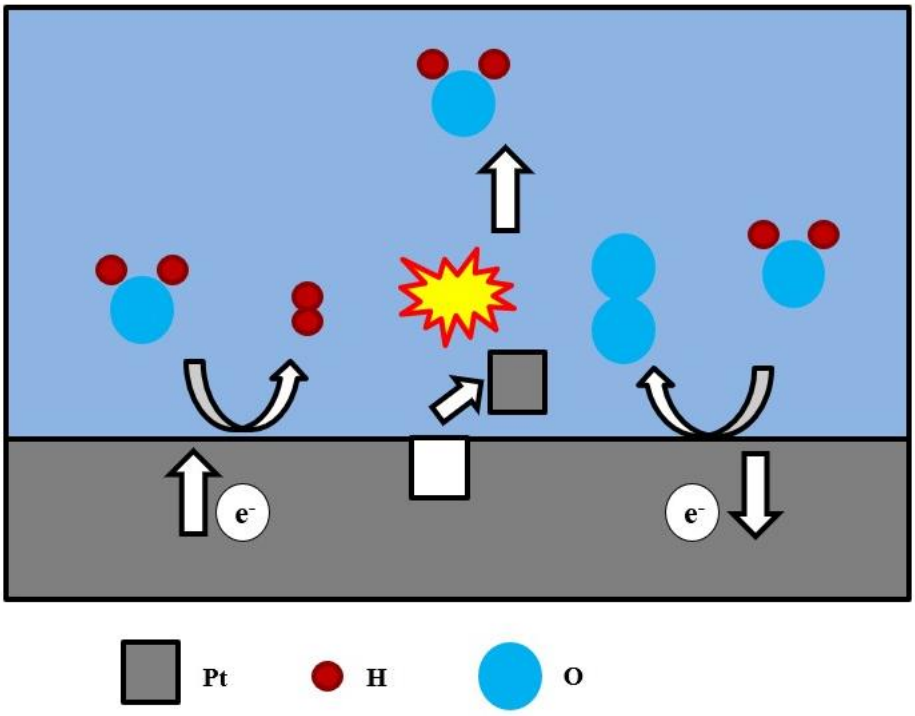

Figure 1.4 The mechanism of micro explosion hypothesis , where hydrogen and oxygen are generated on Pt surface in negative and positive potential sweep. Both bubbles recombine and cause micro-explosion.

Figure 1.5 is the third proposed mechanism of the formation of Pt nanoparticles, which caused by the cation effect. In alkaline electrolytes, K+ cations are diffused to the Pt wire and attack the vacancy on the surface of the Pt electrode during the negative applied potential. In such a high negative potential, the metallic state Pt is reduced to metal anions and they combine with attacking K+ cations into an unstable intermediate transition state. As the potential quickly switches to the positive potential and Pt becomes positively charged, this short lived unstable material leaves the surface of Pt wire with the generation of bubbles and breaks down into the K+ and Pt nanoparticles. The absence of platinum creates more vacancies for K+ cations and maintains the reaction (50).

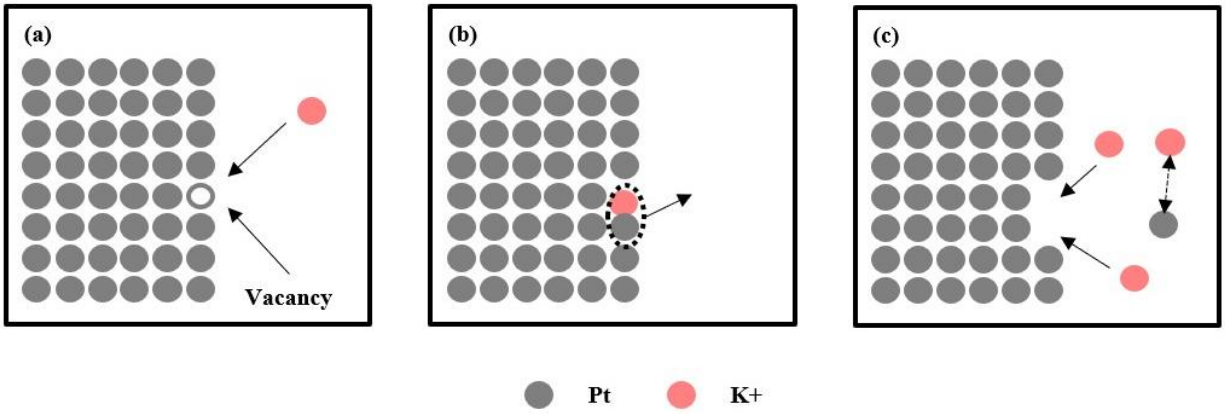

Figure 1.5 The mechanism of cation effect hypothesis, where in a) metal is negatively charged and K+ intercalates into Pt lattice, b) as the potential is increasing and metal surface is positively charged the ejection of meta-stable phase occurs and c) Pt nanoparticles form.

The result of the concentration-effect (33) of the different cations in the electrolyte suggests this theory and the paper in 2009 supports the existence of the metal anions (51). In this paper, we design a series of experiments to identify the mechanism of nanoparticles generation by AC method.

1.4 Valuating the catalyst performance with the electrochemical measurement

For analyzing the nanocatalyst performance, Figure 1.6 provides the design of the 3-electrode setup consisting of the working electrode (WE), the counter electrode (CE), and a reference electrode (RE). The WE is where the desired electrochemical reaction occurs and the potential or current goes through the WE is under control. For electrochemical cell, at least two electrodes are required. In the 2-electrode setup, the CE is the second electrode for conducting current and completing the electric circuit. Connecting the RE to the WE as the third electrode ensures the RE does not participate in the reaction and no current flow to the RE. Since no current passes through the RE, it provides a reference point for measuring or controlling the potential (52).

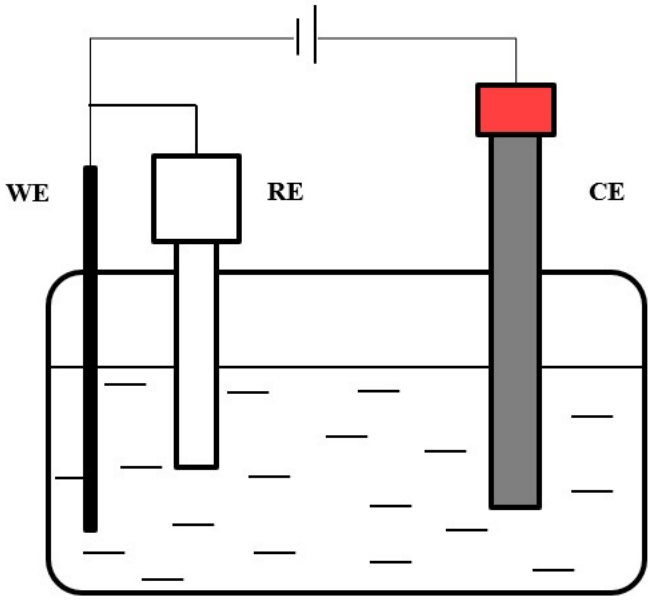

Figure 1.6 The schematic of the three-electrode setup

Figure 1.7 is the design of the Hydro Flex hydrogen reference electrode, which can provide a known, stable potential to measure other potentials. Since no current passed through the RE, it remains at the equilibrium potential, which is well defined. The hydrogen electrode measures the

activity of hydrogen ions directly and very close to 0 V, therefore, no potential correction is needed (52).

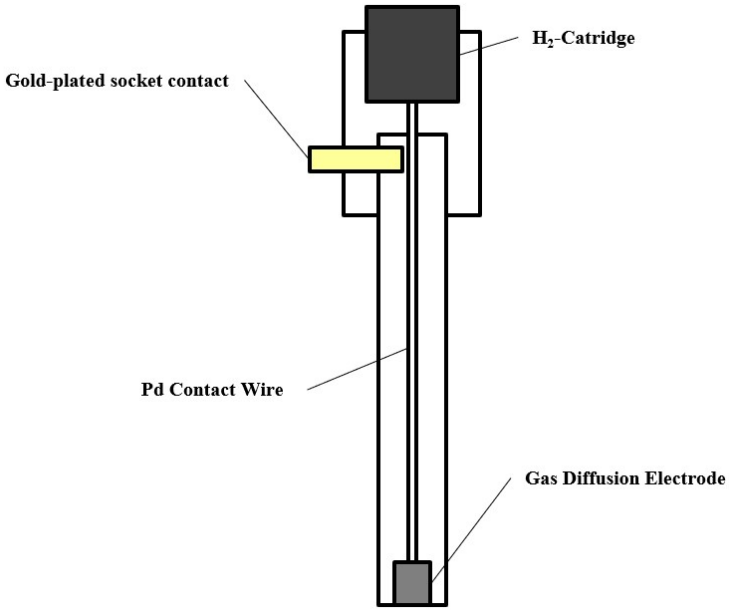

Figure 1.7 The design of Hydro Flex hydrogen reference electrode

The rotating disk electrode (RDE) set up is shown in Figure 1.8. At the end of the rotatable cylinder an electrode disk is embedded, which is surrounded by the insulating material (Teflon). Submerging the RDE into the electrolyte, the velocity of mass-transport to the uniform surface of the disk is distance dependent and is not affected by the radial position or the angle. Since the concentration change of the electrolyte (usually 1 M $HClO_4$) can be neglected and the gas (O_2 or N_2) is pumped in the electrochemical cell with constant speed, the rate of mass-transport does not change with time. The polarization curve is influenced by (1) activation loss, (2) ohmic loss (3) mass-transport and in 3-electrode setup, the last two terms can be removed after the iR-correction, thus, RDE measurements are frequently used in studying ORR and measuring kinetic current (52).

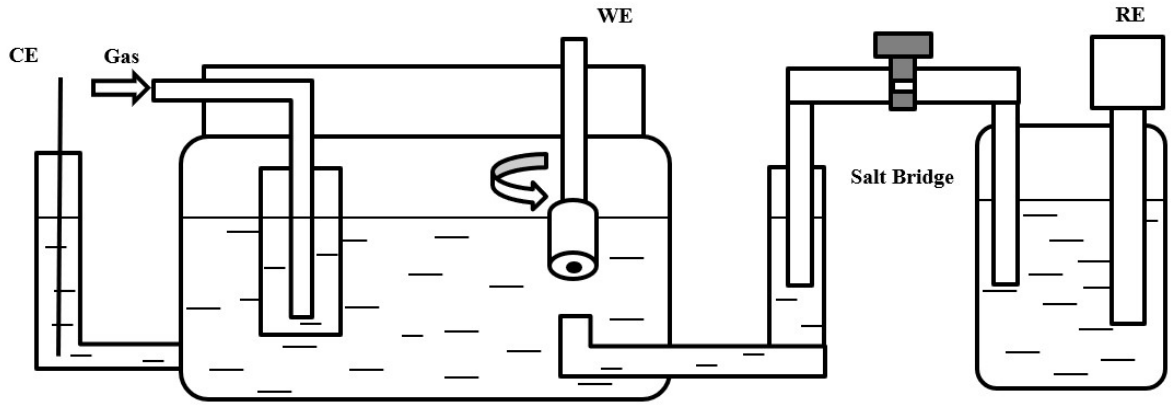

Figure 1.8 The rotating disk electrode measurement set-up, where three-electrode set-up is shown with WE being mounted onto the RDE.

Chapter 2 Methods of Synthesis of Nanoparticles

2.1 Materials and equipment

In this study, four types of wires were used for nanoparticle synthesis. Platinum wire (0.25 mm diameter, 99.9%) and gold wire (0.25 mm, 99.9%) were obtained from Sigma-Aldrich. Palladium wire (0.5mm diameter, 99.9%), and platinum-iridium wire (0.25mm, 99.9% Pt: Ir; 85:15 wt%) were purchased from Alfa-Aesar. Carbon black (Vulcan XC-72R, Fuel Cell Store) was used as a support material. Potassium hydroxide, KOH (Sigma-Aldrich, 85%), potassium chloride, KCl (Sigma-Aldrich, 99.0-100.5%), sulfuric acid, H2SO4 (Sigma-Aldrich, 95.0-98%) and hydrochloric acid, HCl (Millipore Sigma, 1 mol/L) were used as the electrolyte. The 2-Propanol, IPA (Sigma-Aldrich, 99.5%) and Nafion, 5wt% (D521, Fuel Cell Store) were used to prepare ink for RDE testing. Ultrapure water (18.2 MΩ/cm, 3ppb TOC) was generated by Milli-Q Integral water purification system. To obtain cleaned and reproducible conditions, all glassware was washed by ultrapure water at least 3 times before each of the experiments.

VSP potentiostat (Biologic Science Instruments) was used to provide square wave potential. Ultrasonicator (Branson1800) and homogenizer (T25-S1, IKA Labortechnik) were used to disperse and prevented the agglomeration of the nanoparticles during the synthesis. Centrifuge (Ample Scientific, F-33D) was used to separate the nanoparticles in the solution. Laboratory oven (BLUE M) was used to dry the nanoparticles. MSR rotating electrode and standard graphite counter electrode kit for RDE experiment were obtained from Pine Research Instruments. The reference electrode was used hydro flex from Gaskatel. All the TEM images were conducted by the JEM-2800 Transmission Electron Microscope in UC Irvine Materials Research Institute (IMRI).

2.2 Nano platinum catalyst synthesis with 2-electrode setup

In this study, Pt nanoparticles were synthesized in a 20mL vial. This smaller vial was used instead of a large volume beaker since a homogenizer in a smaller beaker enables better carbon black dispersion in the alkaline electrolyte and the Pt distribution on the carbon surface during the synthesis by reducing the distance between two Pt electrodes. As carbon suspension away from electrodes cannot be coated with Pt due to the formation of nanoparticles only near the surface of two electrodes. Besides, the Vulcan carbon with high volatility in the wide-mouth beaker would easily volatilize during the ultrasonic and homogenizing treatment. And since there is no extra space for inserting salt bridge or reference electrode in the 20 mL vial the experiment adopted the 2-electrode setup rather than 3 electrode setup.

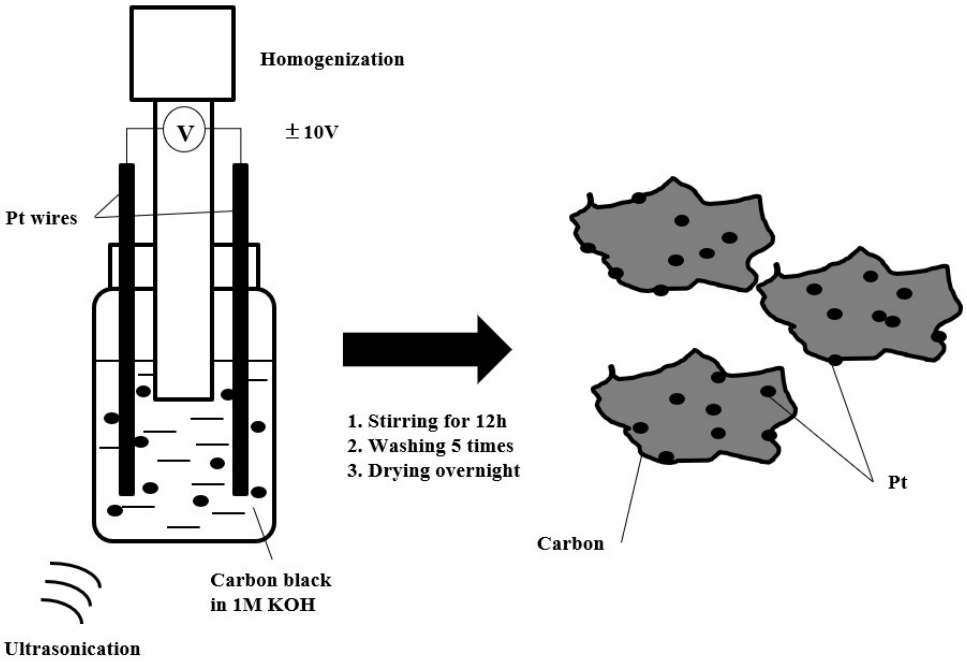

Figure 2.1 Procedure of Nano-Pt synthesizes

For the Pt synthesis 10 mg of carbon was used. The Vulcan carbon with large surface tension is hard to disperse in alkaline solution and it would flow to the top of the electrolyte and it would also aggregate. Thus, before the synthesis, few drops (10 μL each) of 1M KOH were added into the vial with Vulcan carbon and it was stirred until carbon black was completely wet. The procedure was repeated 3-5 times. Then carbon black was filled with 1M KOH solutions of 10 mL and ultrasonicated for 1h with ice water to well disperse the carbon black. As a control case, an additional experiment was conducted without Vulcan carbon. The volume of KOH solution that was added in the vial was same (10 mL) in each experiment since the amount of the Pt nanoparticles generation was affected by the depth that wires immersed into the solution and controlling the amount of electrolyte helps to obtain the desired amount of Pt and the Pt/C ratio.

Before and after each experiment, two metal wires were weighted and then immersed into the solution with 3 cm exposed to the electrolyte. After synthesis, the wires were wiped with Kimwipe, dried, and weighed again. The reaction was fast enough that analytical balance can reflect the difference and the difference in the mass was recorded and was attributed as a mass of nano-particles generation due to the square wave potential applied.

A square wave potential (±10 V 200Hz) was applied to two Pt wires by Biologic for 300s. Compared to sin wave potential, square wave provides a constant potential for both positive and negative charge, which leads to the unchanging reaction speed. Thus, the produced Pt nanoparticles have a small average size and narrow distribution. During the application of high potential, O_2 and H_2 evolve during Pt synthesis on both electrodes rapidly and at the same time, the nanoparticles were generated from the surface of both Pt wires immediately and were dispersed into the whole solution with numerous gas bubbles. To demonstrate the frequency effect on metal particle size, the samples were synthesized in 100/300/400 Hz respectively. To

maximum prevent agglomeration, vials were inserted into the homogenizer and kept in ultrasonicator with ice water during the whole synthesis process. The obtained suspension solution was stirred overnight with a magnetic stirrer to ensure the Pt nanoparticles are fully dispersed on the rough surface of the carbon. The nanoparticles suspension with carbon black was filtered with a vacuum filter and washed with DI water 5 times, while the sample without carbon black was centrifuged at 3300 rpm and washed with DI water 5 times. The sample was dried in the oven at 50℃ for 12h. The synthesis in the ultrasonic bath should fill with ice and the temperature of the oven should not above 80℃ otherwise the Pt nanoparticles would lose catalyst activity which would harm the electrochemistry activity study in the following RDE experiment section(53).

2.3 The preparation of TEM samples

To prepare the sample for TEM, 1 mg of Pt/C nanoparticles was dissolved in IPA. Ultrasonication was performed for 10-30 min until Pt became a uniform and homogenized solution. Cleaning the TEM sample grid by dipping it into the IPA solution for a few seconds. Then drop the nano-Pt solution on the grid and seal it into a box. Standard operation procedure of JEOL 2800 TEM, IMRI was used to operate TEM (54).

2.4 Electrochemical measurement using the rotating disk electrode (RDE)

The RDE experiment was guided by the electrochemical protocol written by Dr. Tristan Asset, a post-doctorate researcher in UCI (53). The cell consisted of two compartments and Luggin capillary. Since the RDE experiment requires an extremely clean environment, thus cleaning was done of the electrochemical cell with a piranha solution (7:3 mixture of concentrated sulfuric

acid and 30% hydrogen peroxide solution) by suspending the cell overnight. Before the start of the experiment, the glassware was washed in boiled water 5 times to completely remove the residue of the piranha solution. For each experiment, the RDE tip was mechanically polished with abrasive paper (2000 and 3000 grit) then polished with three alumina suspension in following order 5 µm, 0.3 µm, and 0.05 µm (3 min each). The suspension was removed by DI water then the tip was cleaned for 5 min in an ultrasonic bath with successive solutions: acetone, ethanol and DI water. The ink contained Pt/C powder, 5 wt% Nafion solution (Ionomer), IPA and DI water and the specific amount of each chemical of the ink is followed:

1. The ratio of Carbon to Ionomer (I) was I/C = 0.3.
2. The ratio of IPA to water was IPA/H_2O = 0.5.
3. The loading of Pt was 20 µg/cm - 40 µg/cm.
4. 10 µL - 20 µL of ink was deposited on the electrode.
5. The surface of the electrode was 0.196 cm^2

Then the rotator was positioned with the tip upwards and rotated at 100 rpm. The ink was gently deposited as rotation rate was slowly increased to 400 rpm. After 30 min the ink was dried, and optically observed for film uniformity then the rotator shaft with tip was immersed into the glass cell. Before the measurements, the 0.1M $HClO_4$ electrolyte was purged with N_2 gas for 15 min. The experiments were collected with the Gamry framework in the following order:

1. The Activation CV was conducted in N_2 gas with a sweep rate of 500 mV/s and the potential range from 0.05 V to 1.23 vs the reference hydrogen electrode, RHE for 100 cycles. The activation was used to clean the surface until the CV from cycle to cycle was overlapping.

2. CV was performed in the same potential at 20 mV/s for 5 cycles in N_2.
3. The LSV was recorded from 0.1 V to 1.05 V vs RHE at 5 mV/s in N_2 and the rotation rate was 1600 rpm.
4. The ohmic resistance was measured by EIS in N_2 with 0.4 V vs RHE, 1 MHz to 1 Hz, 7 points per decade.
5. After purging O_2 for 15 min, LSV was collected with the same condition as step 3 with rotation speed at 400 rpm, 900 rpm, 1600 rpm, 2500 rpm, respectively.

2.5 Mechanism of nanoparticles generation study with 3-electrode setup

The experiment of exploring the phenomenon of the nanoparticle's synthesis was adopted using the 3-electrode setup for the more accurate and precise study of the applied potential effect. Compared to the 2-electrode setup only one metal wire, which served as a working electrode was used in the experiment to have control of applied potential. To study the effect of different metallic elements, several wires (Pt/ Au/ Pd) were used as a working electrode. The counter electrode was graphite with a large surface area. And hydro flex, which is RHE was used as the reference electrode. Hydro flex must be kept in a separate beaker and connected with salt bridge since the reaction would generate nanoparticles and removing the reference electrode from the reaction beaker could prevent contamination.

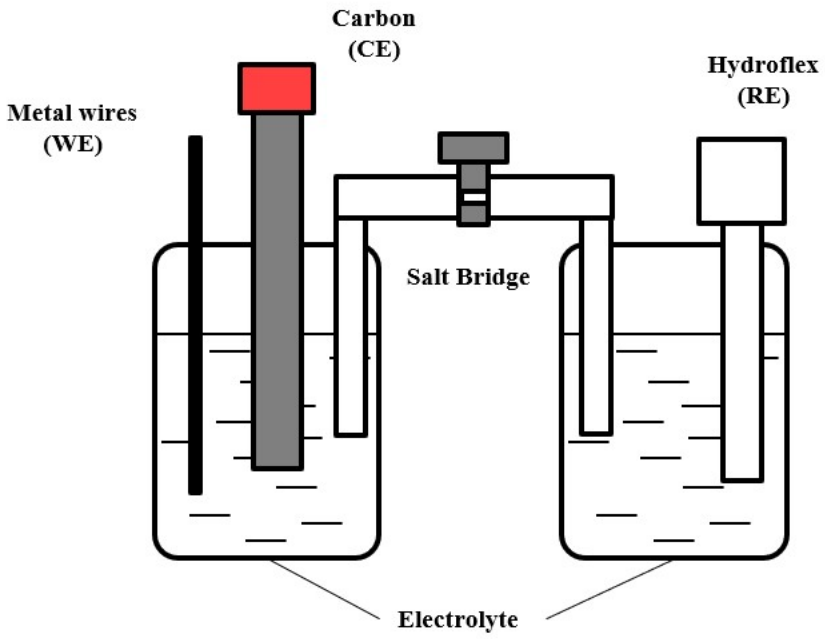

Figure 2.2 Mechanistic study with 3-electrode setup used in this study

To identify the micro explosion theory, N_2 was purged for 15 min before each experiment to minimize the effect of the O_2, which dissolved in the electrolyte. For studying the mechanism of nanoparticles generation, no support material was added into the electrolyte since the transparent solution without Vulcan carbon would contribute to observing the generation of particles. In this study, the mass loss of Pt wire before and after the synthesis was measured by analytical balances. Hence, adequate reaction time was essential to reflect the mass difference in the balances. And the reaction time was determined by the repeat cycles. Since all the experiments for the mechanism, the study was conducted in 200 Hz, and the repeat cycles in 5 min would be 60,000.

Several groups of experiments were conducted in various conditions (metal/electrolyte/potential) and details are listed in the next chapter.

Chapter 3 Results

3.1 The carbon effect during the synthesis

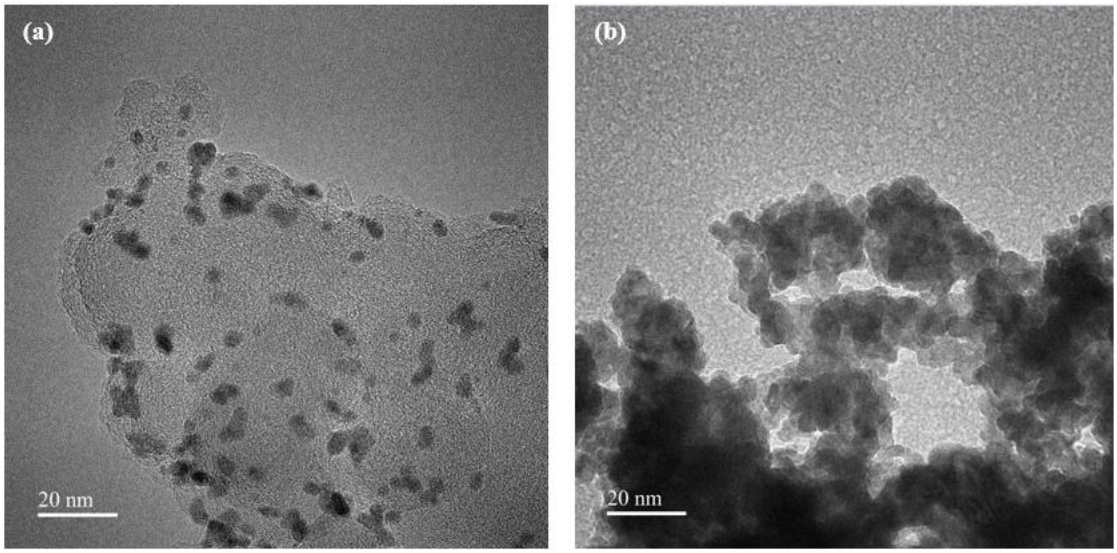

Figure 3.1 (a) Pt nanoparticles with Vulcan carbon black as support and (b) Pt nanoparticles without Vulcan carbon.

Figure 3.1 (a) and (b) show two representative TEM images of nanostructured Pt particles with and without the support of Vulcan carbon, respectively, prepared by the alternating current method. The dark particles in Figure 3.1(a) are Pt nanoparticles and the large grey cloud in the image is carbon black that was added to the solution before the synthesis to disperse Pt nanoparticles and for later electrochemistry activity measurements. Apparently, adding the porous Vulcan carbon as a support material can tremendously enhance the dispersity and reduce the Pt particle aggregation. Besides, the method of separating the particles from the carbon black suspension after the experiment would affect this conclusion since for the shape of the sample without Vulcan carbon were more like hydrosol thus the pore size of the vacuum filter paper were not small enough to separate the particle and the particles might be aggregated during the

centrifuge process. Pt nanoparticles will agglomerate without added surfactant, as shown in Figure 3b.

3.2 The impact of frequency on the particle size

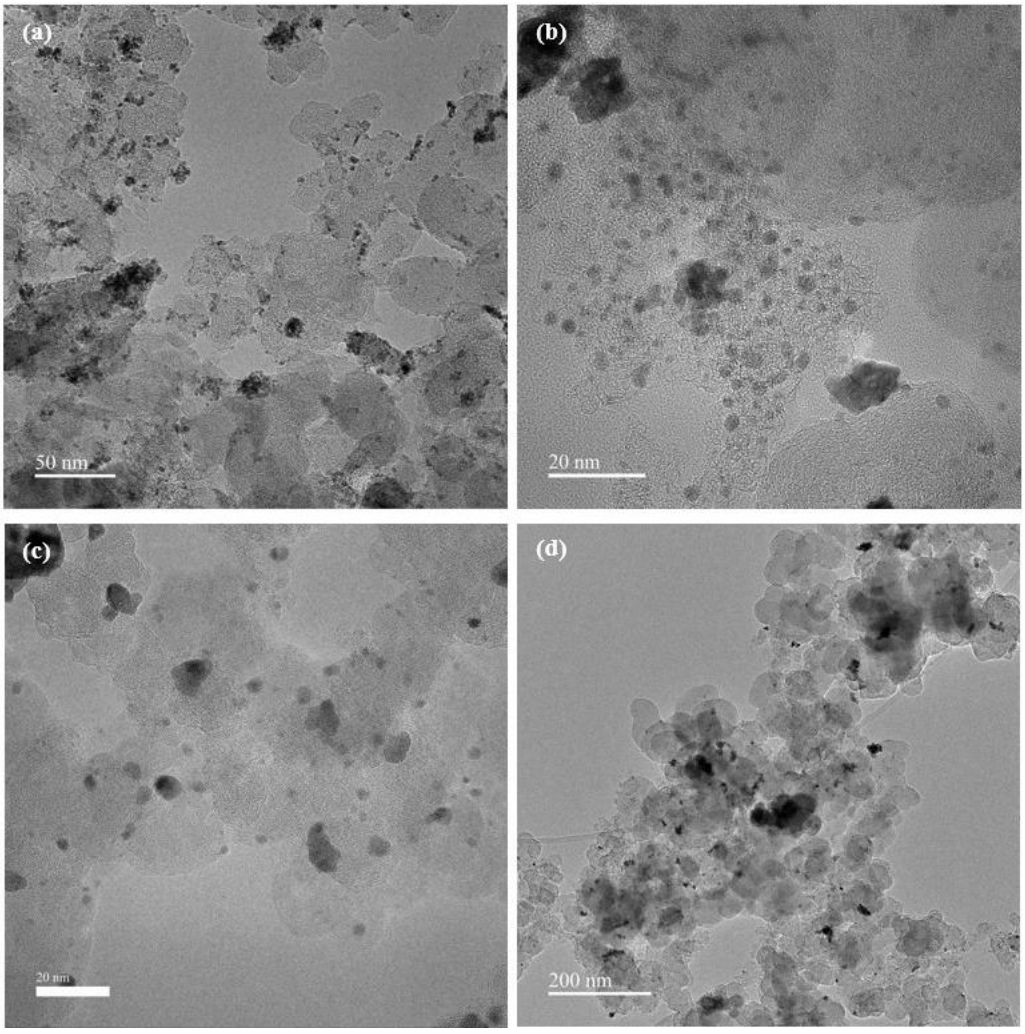

Figure 3.2 TEM images of Pt particles synthesized using AC frequencies of (a) 100 Hz (b) 200 Hz (c) 300 Hz (d) 400 Hz

The typical TEM images of Pt/C synthesized with varied AC frequency of 100 – 400 Hz are shown in Figure 3.2. In Figure 3.2, round-shaped Pt nanoparticles below 10 nm in size were synthesized by applying square wave potential. Pt nanoparticles were unevenly dispersed on the

surface of the Vulcan carbon and some of the particles were aggregated together. Besides, we observe carbon particles without Pt nanoparticles, and this can explain by the hydrophobicity of the Vulcan carbon. Some carbon particles were flowing on top of the alkaline solution inevitably and were not involved in the synthesis process but were collected by the filtration. And the carbon that dispersed into the solution with distancing to the Pt wire would reduce the opportunity to interact with newly synthesized Pt particles.

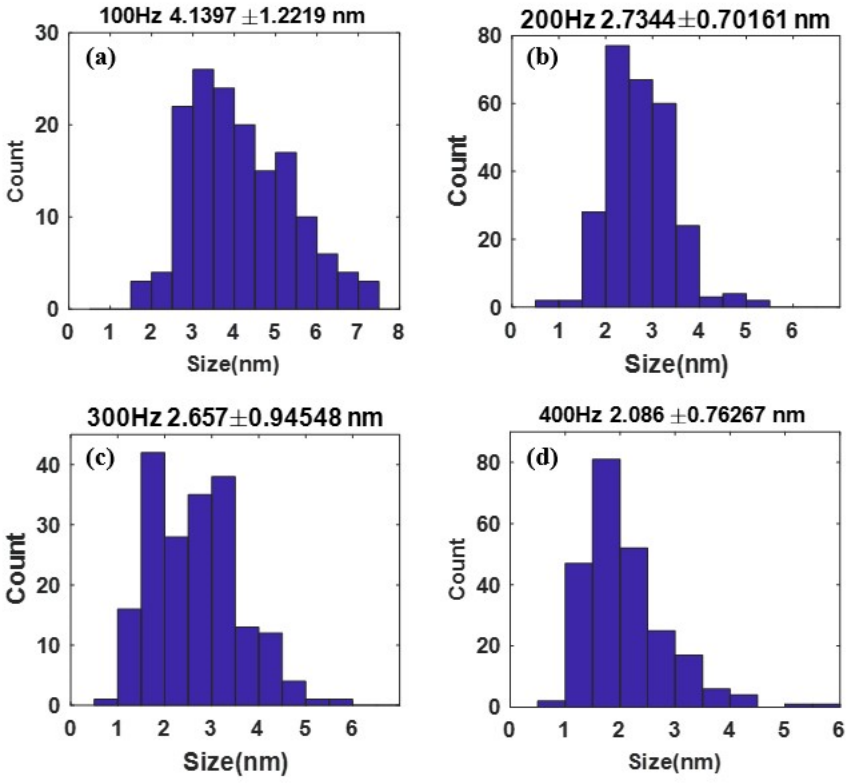

Figure 3.3 Size distribution of Pt particles synthesized using various frequencies (a) 100Hz (b) 200Hz (c) 300Hz and (d) 400Hz.

Figure 3.3 shows the particle size analysis of Pt from TEM images reported in Figure 3.2 with ImageJ. For each set of frequency, over 100 particles were measured using different TEM

images. The distribution chart reveals the number averaged sized for Pt/C nanoparticles is 4.14 ± 1.22 nm (100 Hz); 2.73 ± 0.70 nm (200 Hz); 2.66 ± 0.95 nm (300 Hz); 2.09 ± 0.76 nm (400 Hz). Ideally, the narrow Pt size-distribution is preferred, as it enables control and reproducibility. The standard deviation of the distribution reports the spread of Pt nanoparticles sizes for each frequency. Pt nanoparticles synthesized at 100 Hz has the broadest distribution with a standard deviation of 1.22 nm. The Pt particles synthesized at higher frequencies have lower spread. Thus, synthesis with 100 Hz is not as desirable, as it does not allow control over the size.

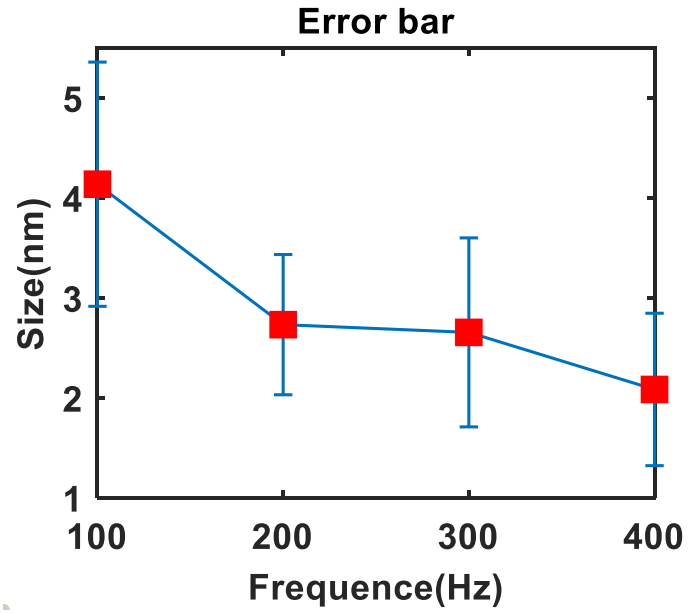

Figure 3.4 Dependence of synthesized Pt nanoparticles size on synthesis AC frequency

Figure 3.3 and Figure 3.4 show as the AC frequency increases, the particle size of Pt decrease from 4.14 nm to 2.09 nm and compare to the particle size in 100 Hz and 400 Hz, the size distribution was narrower from 1.22 nm to 0.76 nm. Since the Pt nanoparticles were formed in every potential shift cycle, increasing the frequency would reduce the time for the growth of

nanoparticles before detachment. Therefore, a clear trend is observed in Pt-size with respect to AC synthesis frequency.

3.3 The electrochemical performance from RDE analysis

The cyclic voltammetry (CV) is used to analyze the oxidation and reduction processes, as well as to measure an electrochemical surface area (ECSA) of Pt. To generate the CV curve, a triangle wave potential is applied. In this experiment, the potential increased from 0.05 V to 1.23 V at 20 mV/s scan rate, which called anodic scan, and the cathodic scan was decreased from 1.23 V to 0.05 V at the same velocity (vs RHE). The anodic scan and the cathodic scan constitute a complete cycle. In the anodic scan, the oxidation reactions occur. According to the standard potential of the half-reaction of hydrogen and oxygen, in 1 M $HClO_4$, hydrogen oxidize to ionic state combined with Pt catalyst in the low potential region (0.05 V to 0.4 V vs RHE) and oxygen is formed in the high potential region (1 V to 1.23 V vs RHE). While in cathodic scan the reduction reaction occurs. Hydrogen is formed in the low potential region and the oxygen is consumed in the high potential region. Under the sweep cycle of 0.05 V to 1.23 V triangle potential, the oxidation current and the reduction current response in the anodic scan and cathodic scan, respectively, and the CV cure is obtained. (52,55) The CV curve for four different frequencies are shown in Figure 3.5.

Typically, the catalyst activity of Pt nanoparticles, synthesized with the AC method, depends on the surface area of nanoparticles. The hydrogen peak increased from 100 Hz to 300Hz. However, with the smallest size nanoparticles, the sample generated with 400 Hz has a low hydrogen oxidation peak, which might be due to the carbon corrosion at 0.75 V (56).

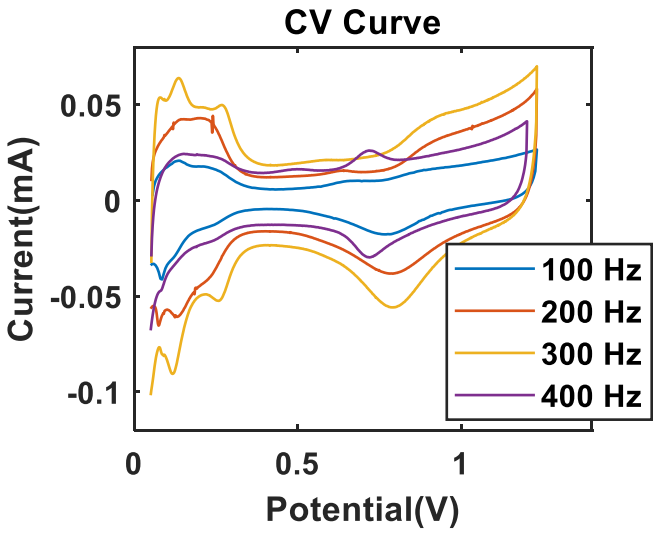

Figure 3.5 CV curves for Pt/C samples synthesized at various frequencies for 100 to 400 Hz.

Since Pt catalyst accelerates the redox half-reactions, the activity of platinum nanoparticles is generally proportional to the electrochemical surface area (ECSA), which can be measured quantitively by integrating current in the Hupd region. The ECSA is used for analyses the surface area of platinum catalyst and the equation for calculating ECSA is below (53):

$$ECSA_{Pt}(m^2 g_{Pt}^{-1}) = \left[\frac{Q_H(C)}{210(\mu C cm_{Pt}^{-2}) * m_{Pt}(g)}\right] * 10^5$$

$$\text{Charge } Q_H(C) = \frac{Peak\ area(V \cdot A)}{Scan\ rate(V/t)}$$

Where $Q_H(C)$ is the charge in the hydrogen adsorption region, which is obtained from the integral of the hydrogen oxidation peak in the CV curve and divided by scan rate. The constant is the charge of monolayer adsorption of protons to a surface of polycrystalline platinum (53) and m_{Pt} is the loading of Pt on the electrode disk. Typically, the ECSA is higher for reduction scan rather than the oxidation scan. Table 3.1 includes oxidation ECSA and reduction ECSA from frequency of 100 Hz to 400 Hz. Since the Vulcan carbon was added before the synthesis of Pt

catalyst for better dispersion, the Pt/C loading was different in 4 samples. The sample synthesized with 100 Hz has 19.98 m^2/g_{Pt} oxidation ECSA and the low ECSA might due to the Pt agglomeration. The oxidation ECSA and reduction ECSA for sample with 200 Hz are 30.07 m^2/g_{Pt} and 24.3 m^2/g_{Pt}, respectively. While the oxidation ECSA and reduction ECSA for samples in 300 Hz are 25.81 m^2/g_{Pt} and 32.19 m^2/g_{Pt}. Due to the carbon corrosion, the sample in 400 Hz with 20 μL, which is double than any other sample, has only 5.96 m^2/g_{Pt} oxidation ECSA and 15.08 m^2/g_{Pt} reduction ECSA.

Table 3.1 The ECSA in the sample synthesized by various frequencies

Frequency (Hz)	**Ink volume (μL)**	**Loading (Pt/C)**	**Oxi ECSA ($m^2 g_{Pt}^{-1}$)**	**Red ECSA ($m^2 g_{Pt}^{-1}$)**
100	10	17%	19.98	30.96
200	10	31%	30.07	24.3
300	10	23%	25.81	32.19
400	20	17%	5.96	15.08

The electrochemical impedance spectroscopy (EIS) is the method to investigate the resistance of an electrochemical system (52). A typical Nyquist plot is combined with a semi-cycle and a straight line with a slope of 1, which is shown in Figure 3.6. The frequency decreases along the x-axis. In high frequency, the semi-cycle can be regarded as an AC circuit while the 45-degree straight line in low frequency can be seen as DC circuit. And the intersect of the semi-cycle and the straight line is the resistance of the electrochemical cell. The resistance of 4 cells is listed in

Table 3.2. The resistance of the RDE cell is for iR-correction and should below 30 Ω, thus we select the samples generated with 200 Hz and 300 Hz and do further analysis.

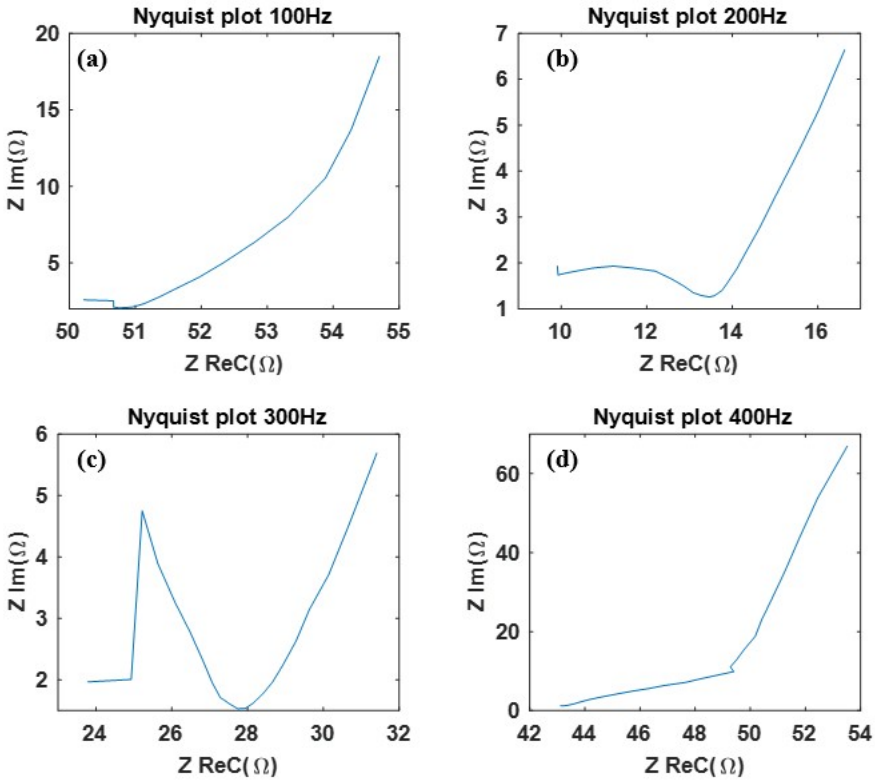

Figure 3.6 Nyquist plots in the sample Pt/C synthesized with various frequencies (a) 100Hz (b) 200Hz (c) 300Hz (d) 400Hz.

Table 3.2 The high-frequency resistance of the electrochemical cell for 4 samples.

Frequency (Hz)	100	200	300	400
Resistance (Ω)	51	14	28	49

For linear sweep voltammetry (LSV), only the anodic scan is applied and the potential increase from 0.1 V to 1.05 V. Figure 3.7 shows the LSV plot for 400, 900, 1600 and 2500 rpm, respectively. The halfway potential are listed in Table 3.3. For the 200 Hz sample, the halfway potentials are 916, 905, 898, 895 mV in 400, 900, 1600, 2500 rpm, respectively. While the 300 Hz sample has 931, 922, 913, 906 mV halfway potential in 400, 900, 1600 and 2500 rpm, respectively.

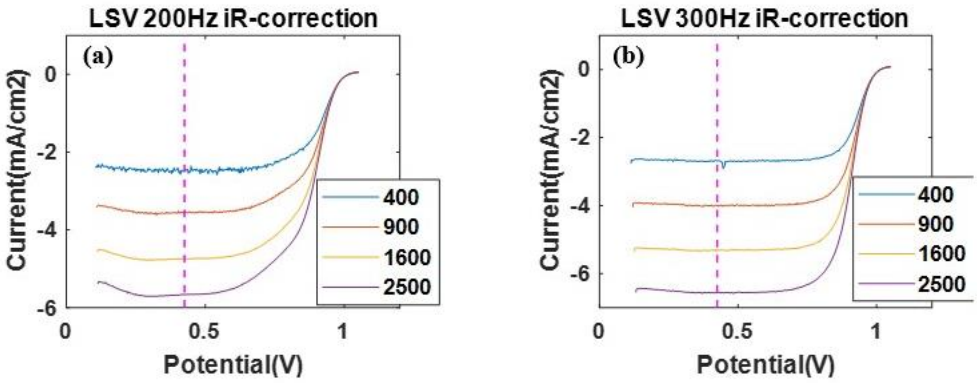

Figure 3.7 the LSV plot with iR-correction (a) 200Hz (b) 300Hz

Table 3.3 The halfway potential from LSV plot

rpm	½ E (mV) in 200 Hz	½ E (mV) in 300 Hz
400	916	931
900	905	922
1600	898	913
2500	895	906

The LSV curve at 1600 rpm was used to calculate kinetic current (i_k) by Koutecky-Levich equation (57):

$$\frac{1}{i_m} = \frac{1}{i_k} + \frac{1}{B_L} \cdot \frac{1}{\sqrt{\omega}}$$

i_m is the measured current (mA/cm^2)

i_k is the kinetic current (mA/cm^2)

ω is the angular rotation rate of the electrode (rad/s)

B_L is the Levich Constant

$$B_L = 0.620nFD^{\frac{2}{3}}\nu^{-\frac{1}{6}}C$$

n is the number of moles of electrons transferred in the half-reaction

F is the Faraday constant (C/mol) F=96485 C mol^{-1}

D is the diffusion coefficient (see Fick's law of diffusion) (cm^2/s) $D_{O2}=2.1*10^{-5}$ cm^2s^{-1}

v is the kinematic viscosity (cm^2/s) v=0.0107 cm^2s^{-1}

C is the analyte concentration (mol/cm^3) $C_{O2}=1.03*10^{-6}$ mol cm^{-3}

The Koutecky-Levich plot is shown in Figure 3.8. The intersect of the plot ($1/i_k$) can directly read from the plot, which is 0.0278 and 0.0054 cm^2mA^{-1} for samples in 200 Hz and 300Hz, respectively. The slop of the plot represents one over the Levich constant and is used for calculating the number of electrons transferred in the half-reaction. The value of n is 4.13 and 4.21 confirming the four-electron pathway.

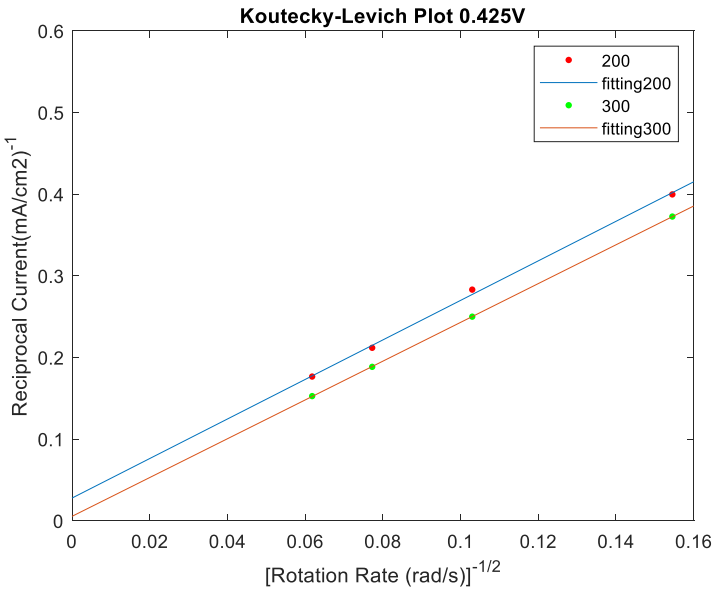

Figure 3.8 KL plot for Pt/C generated with 200 and 300 Hz AC method.

The kinetic current density, the mass activity (MA), and the specific activity (SA) are shown in Table 3.4. The geometric surface area of the rotating disk electrode is 0.196 cm^2 and the kinetic current density is the reciprocal of the intersect, which is 35.97 and 185.19 $mAcm^{-2}$, respectively. The Pt loading on the electrode disk is 40 µgPt /cm^2 and the current at 0.9 V was used for iR-correction. The equation of MA and SA is followed:

$$MA = \frac{i_k}{Pt\ loading}$$

$$SA = \frac{i_k}{ECSA}$$

Table 3.4 The electrochemical activity of synthesized Pt catalyst

Frequency (Hz)	Potential (V)	Slope 1/B ($cm^2A^{-1}rad^{1/2}$)	Intercept $1/i_k$ (cm^2mA^{-1})	i_k ($mAcm^{-2}$)	n	MA (mA/mg_{Pt})	SA ($\mu A/cm^2_{Pt}$)
200	0.425	2420.9	0.0278	35.97	4.13	899.25	1196.21
300	0.425	2375.4	0.0054	185.19	4.21	4629.75	7175.13

3.4 Critical potential range for nanoparticles generation

According to the micro explosion theory, (49) the nanoparticles were the byproduct during the combustion of hydrogen and oxygen, which were generated in hydrogen evolution reaction (HER) and oxygen evolution reaction (OER). Thus, producing hydrogen and oxygen simultaneously is essential for the micro explosion theory. To test this hypothesis, an overpotential was applied to two half-reactions to ensure the formation of two gases. And the standard electrode potential of HER and OER vs RHE (21) are listed below:

$$2H^+ + 2e^- \rightarrow H_2 \qquad 0\ V$$

$$O_2 + 4H^+ + 4e^- \rightarrow 2H_2O \qquad 1.23\ V$$

The experiments in Table 3.5 were conducted in 1 M KOH, at 200 Hz frequency. The generation of nanoparticles can be simply distinguished by the change of color of the solution. In the 1 M KOH transparent solution, the generation of Pt nanoparticles could disperse with bubbles and turn electrolyte to a black hydrosol in less than 1 min.

Table 3.5 Applying different set of alternating potential to Pt wire in 1 M KOH

Over potential	Negative potential	Positive potential	Nanoparticles	Mass loss (mg/min)	Time (min)
1	-1	2.23	No	0.22	5
1.2	-1.2	2.43	No	0.12	5
-1;2	-1	3.23	No	0.28	5
-2;1	-2	2.23	No	0	5
1.5	-1.5	2.73	Yes	1.04	5
1.7	-1.7	2.93	Yes	0.97	3
2	-2	3.23	Yes	0.97	3
3	-3	4.23	Yes	1.7	1

Several sets of overpotential were applied to the Pt wire in the 3-electrode setup as shown in Figure 3.9. The nanoparticles started to form at 1.5 V overpotential. The potential on the WE alternated between –1.5 V and 2.73 V. At -1.5 V HER occurred, whereas at 2.73 V OER occurred. Pt nanoparticles were systematically synthesized above this critical overpotential and the mass loss per min was around 1 mg from 1.5 V to 2 V overpotential, but as the overpotential increased to 3 V, the mass loss increased to 1.7 mg. During the experiment, the difference in reaction rate was observed. At 1.5 V overpotential, bubbles and nanoparticles were slowly released from the Pt wire and after 5 min of the experiment, the grey hydrosol was flowing on the transparent KOH electrolyte, while the generation rate was significantly increased in 3 V and the solution turn to the uniform black ink in 1 min.

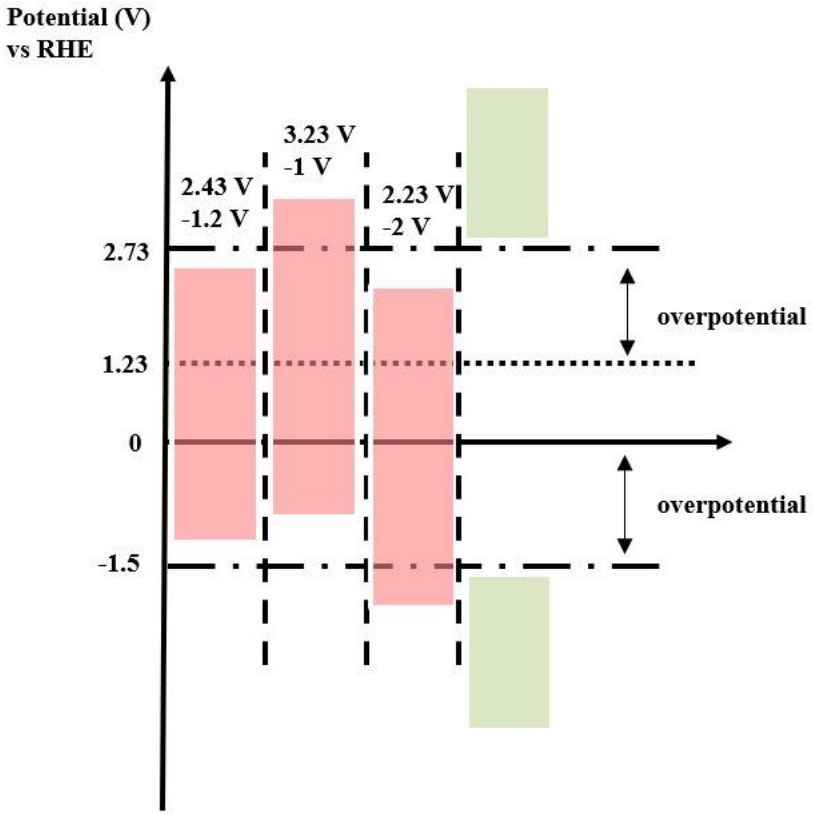

Figure 3.9 The critical potential for the generation of Pt nanoparticles

Pt nanoparticles would not form below 1.5 V; bubbles came out and we did not observe any visible nanoparticle and the metallic Pt wire turned black. However, a small mass loss from 0.12 mg to 0.22 mg occurred without particle formation. Platinum might dissolve into the solution in the ionic state during these high applied potentials.

Besides, in Table 3.1, uneven overpotential showed the same observation. Applying -1 and 3.23 V or -2 and 2.23 V alternating potential on a WE did not synthesize the Pt nanoparticles. In these two cases, one of the overpotentials was above 1.5V and one was below this critical potential, which means the nanoparticles can only exist when both negative and positive potential on the

WE were above 1.5 V. Also, no mass loss in -2 and 2.23 V can be explained the dissolution of Pt would inhibit as two potential were close.

Moreover, researchers claimed particles can be synthesis by only applying a negative alternating potential (25–30,40) while we cannot repeat the results reported in those works. The generation of hydrogen and oxygen simultaneously was necessary. By controlling the potential that only formed one of the two gases (hydrogen or oxygen) would not trigger the formation of Pt nanoparticles. In -10 and 0 V, only the hydrogen was formed and in 0 and 10V only oxygen was formed, and we did not observe Pt nanoparticles in these two regimes.

3.5 The concentration of cation contributing to the synthesis of nanoparticles

To identify the short-lived cation effect (50), the concentration of potassium cations was controlled during each synthesis experiment. The potassium chloride powder was added to increase the concentration without changing the volume of the solution and the pH of the electrolyte. In Figure 3.10, a 200 Hz square wave potential (5.23 V to -4 V) was applied to the Pt wire for 3 min in the 70 mL 1 M KOH solution. As the concentration of K+ increased from 1 M to 2 M, the reaction was accelerated, and the mass-loss rate increased from 1.63 mg/min to 2.33 mg/min.

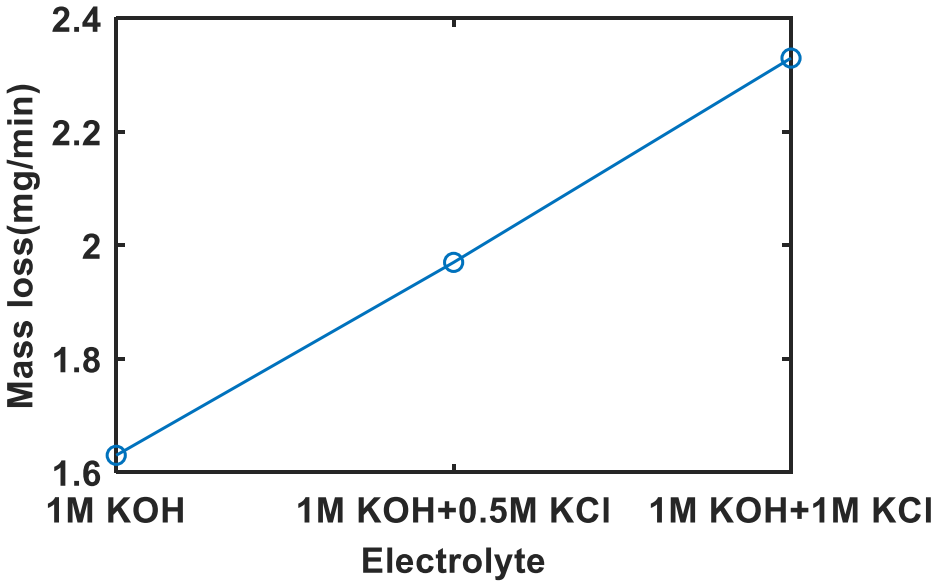

Figure 3.10 Mass loss in different concentration of K+ anion

Since chloride ions were added to the system, Cl_2 was formed as a byproduct instead of O_2. This experiment proved the nanoparticles can be synthesized without the presence of oxygen, thus the micro explosion theory was less likely to be the mechanism of particle synthesis.

3.6 The novel method to synthesize Pt nanoparticles in the neutral and acid electrolyte

Many researchers reported the platinum nanoparticles synthesis in alkaline media using the AC method (22,32,33,36,38–40,42,44) but none of the works were able to synthesize Pt nanoparticles in the neutral or acid media. According to the K+ cation effect theory, Pt particles should be synthesized in neutral or acid media with the presence of K+ ion. In Table 3.2 and Table 3.3, experiments were conducted in the 3-electrode setup with 200 Hz square wave potential and this is the first-ever work to observe the Pt particle generation in pH < 7.

Table 3.6 Pt nanoparticles synthesized in 1 M KCl solution.

Electrode	Potential (V)	Nanoparticles	Mass loss (mg/min)	Time (min)
Pt wire + Carbon	5.23; -4	Yes	0.9	3
2 Pt wire	5.23; -4	Yes	0.4	3

As shown in Table 3.6, particles were synthesized in neutral 1 M KCl electrolyte. Pt wire and carbon electrode were adopted as working electrode and counter electrode, respectively. During the 3 min +5.23 and -4 V square wave potential period, 0.9 mg nanoparticles were generated per minute, while the counter electrode switched to the Pt wire, the mass loss dropped to 0.4 mg/min from a single wire. In the same condition, 2 Pt wire setup produced fewer Pt nanoparticles than 1 Pt wire setup thus the color of the solution after the experiment was significantly lighter. It might be because the surface area of the carbon electrode was larger than the thin Pt wire. With a larger surface, more current pass through the electrode and would generate more nanoparticles.

Besides, as two Pt wires in the electrolyte moving closer, the rate of bubbles generation increase due to the decrease of the ohmic resistance of the system. Therefore, the distance between two electrodes, the volume of electrolytes, and the immersed depth of the electrode should be constant in each set of experiments.

Table 3.7 Pt nanoparticles synthesized in different pH

pH	Electrolyte (1 M)	Potential (V)	Nanoparticles	Mass loss (mg/min)	Time (min)
0	80 mL HCl	±6	No	0	3
5.35	80 mL KCl + 0 µL HCl	±6	Yes	0.97	3
3.22	80 mL KCl + 50 µL HCl	±6	Yes	0.7	3
2.5	80 mL KCl + 400 µL HCl	±6	Yes	0.6	3
1.42	80 mL KCl + 5 mL HCl	±6	Yes	0.6	3
0.9	80 mL KCl + 20 mL HCl	±6	Yes	0.6	3

In Table 3.7, no particle were formed in 1 M HCl solution. However, nanoparticles formed in the acid electrolyte when K+ ions were present. The various volume of the 1 M HCl solution was mixed with the 1 M KCl solution. Pt nanoparticles were still synthesized as the pH dropped from 5.35 to 0.9 while the mass loss rate was decreased from 0.97 mg/min to 0.6 mg/min. Compared with the results in alkaline solution, the average response current for synthesized nanoparticles was dropped from 3A to 0.6A, which reflected the reduced reaction rate and reduced amount of Pt produced.

Surprisingly, compared with neutral media, applying 5.23 V and -4 V square wave potential in KCl and HCl acidic mixture did not generate particles, only at higher potentials (±6) nanoparticles were generated. This contradictory phenomenon can be explained by ionic mobility. The ion mobility of K+ and H+ in water is 7.62 and 36.23 (µ)/10^{-8} m^2 s^{-1} V^{-1} respectively and the relative mobility (relative to K+) of H+ was 4.75 (58). When applying the

negative potential to the Pt wire below its potential zero charge (~0.23 V) high mobility H+ ions with smaller volume would reach the surface of the electrode before K+ ions. In acidic electrolyte, the consumption rate of protons in hydrogen evolution reaction was slower than the H+ ion mobility thus, H+ ions absorb onto Pt surface and blocking the K+ intercalation into a platinum wire. Therefore, an extra negative potential will be required to overcome the Pt-H double-layer capacitance.

In lower pH, as the concentration of H+ increased, the lower generation rate of bubbles and particles were observed. In Figure 3.11, the mass-loss rate decreased as the pH dropped from 5.35 to 2.5 but no significant difference in reaction rate was observed after more than 400 µL HCl was added into the beaker. It might be because the concentration of H+ reached the critical value and no longer affect the reaction-rate.

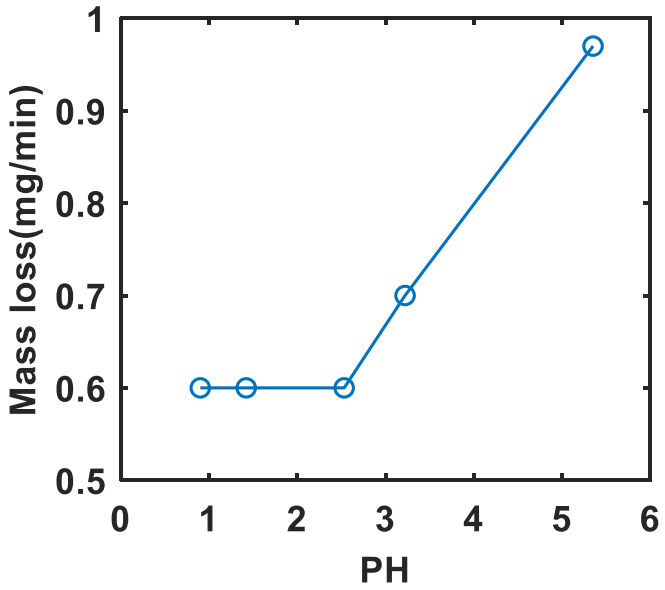

Figure 3.11 Mass loss in different pH

The sample for TEM imaging in Figure 3.12 was synthesized in the acidic electrolyte (60 mL KCl + 20 mL HCl, pH 0.8) and ±6 V 200 Hz square wave potential was applied to the Pt wire in a 3-electrode set up in a glass cell with the salt bridge. 20 mg of Vulcan carbon XC72 was added to the electrolyte before the experiment and 4.9 mg of Pt nanoparticles were produced in 30 min. The nanoparticles were centrifuged 3 times with 4500 RPM.

In Figure 3.12 (b), the long thin shape of Vulcan carbon black suggests carbon corrosion (59) during the synthesis in acidic electrolyte. The polygon shape, cylindrical shape and oval shape of Pt nanoparticles are found in Figure 3.12 (c) - (e). Figure 3.12 (f) shows the disordered orientation of platinum on Vulcan carbon.

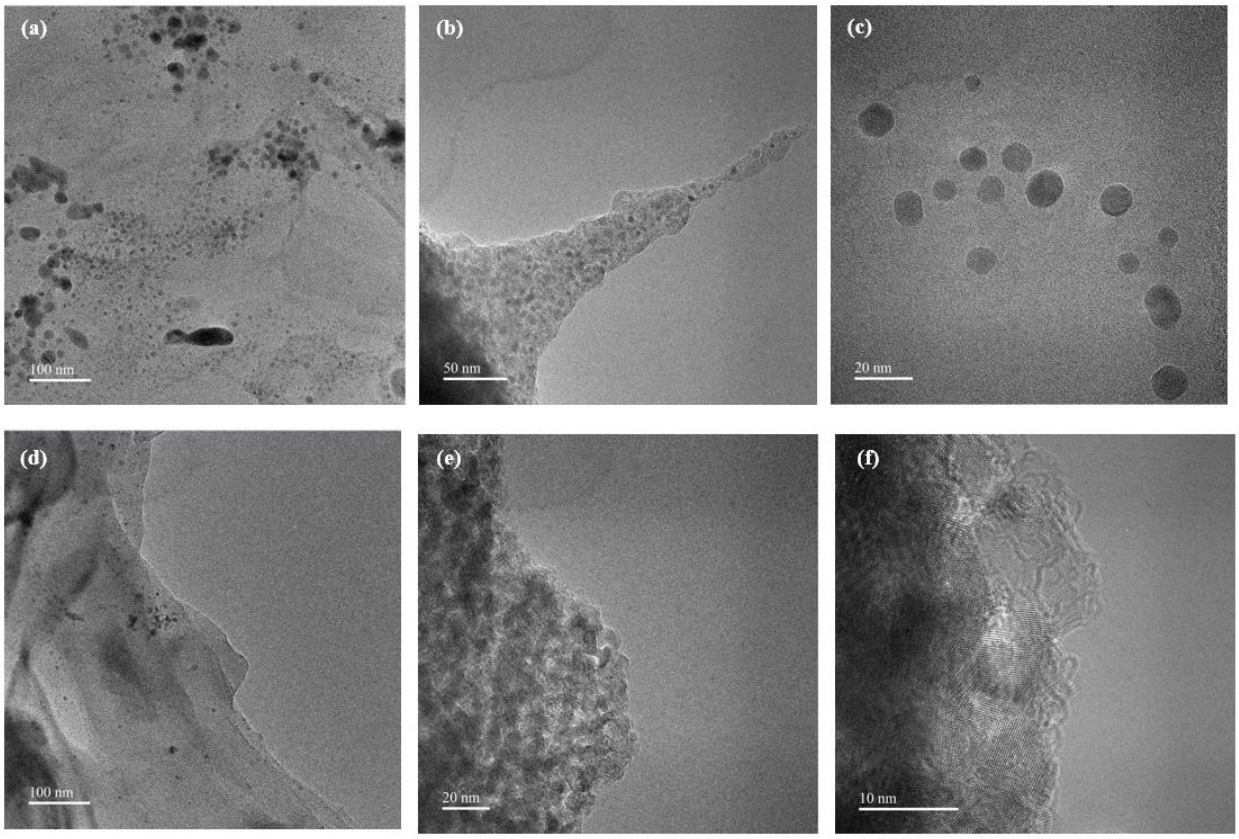

Figure 3.12 TEM image of platinum nanoparticles synthesized in acid

Comparing these TEM images with the TEM image in the alkaline electrolyte in Figure 3.2, the bad dispersion and ununiform shape of platinum in Figure 3.12 is caused by the difficulty of measuring the Pt nanoparticles size. In alkaline solution, platinum nanoparticles are round in shape, while in HCl and KCl mixture, various type of shapes is unevenly spread on the carbon support. For alkaline media, Pt was synthesized in a vial with 2-electrode setup, the small container has better carbon dispersion and shapes control while platinum nanoparticles in acid were synthesis in a large glass cell with the salt bridge, most of the solution (HCl + KCl with carbon) between WE and CE did not contribute to the synthesis. For quantifying the nanoparticle shapes in neutral and acidic solutions, further experiments are required.

3.7 The alternating current method for synthesis of Au and Pd nanoparticles

For better understanding the mechanisms of the generation of nanoparticles, other metal wires apart from platinum were used. The same square wave potential in the 3-electrode setup was applied. In the McCann et al. paper (47), Au nanoparticles were synthesized in the neutral electrolyte by applying the AC potential, however, as shown in Table 3.8, no Au nanoparticle were formed in alkaline/ neutral/ acid electrolyte when we attempted the synthesis in a wide potential window.

In KOH and KCl electrolytes, no mass was lost after 3 min of AC potential application. We observed bubbles generation in this potential regime. On the surface of the Au wire, the red gold oxide (Au_2O_3) was formed during the synthesis procedure. It was not possible to remove by wiping the wire with tissue paper, as we did with Pt wire. Since the non-symmetric potential was applied, Au_2O_3 also formed on the carbon electrode in the electroplating process. A significant heat was also produced during the experiment with Au wire compared to the Pt experiment. The

whole gold wire was completely dissolved in the 1M HCl solution and turned to a yellow solution ($AuCl_3$). At 4 V overpotential, 15 mg/min gold was rapidly dissolved in 1 M HCl, in comparison, 1.63 mg/min, 0.97 mg/min, and 0 mg/min of platinum were lost in the KOH, KCl, and HCl, respectively, in the same condition.

Besides, a trial with Pd wire was conducted at ± 6 V 200 Hz square wave potential in 1 M KCl, and we successfully produced palladium nanoparticles.

Table 3.8 Au wire in 3-electrode setup with 200 Hz square wave potential

Electrolyte	Potential (V)	Nanoparticles	Mass loss (mg/min)	Time (min)
1 M KOH	5.23; -4	No	0	3
1 M KCl	5.23; -4	No	0	3
1 M HCl	5.23; -4	No	15	3

The metal oxide was formed in high AC potential (41,48), for the gold experiment, the gold (III) oxide coated on the surface of the electrode tightly and the prohibited the dissolution in KOH electrolyte, while the Au_2O_3 was soluble in acid and did not trigger the passivation process. Also, the insoluble platinum oxide in acid passivated particles generation in 1M HCl and the dissolution of PtO lost the ability to protect the wire from the generation of nanoparticles.

Chapter 4 Conclusion

In conclusion, we successfully synthesized the Pt nanoparticles within sizes of 2 – 5 nm with the alternating current method and first reported the Pt generation in pH < 7. For the three mechanism theories, we have a proof for the cation effect hypothesis, since the corrosion hypothesis was unable to explain particles formation from the alloy wire that retained alloy structure as nanoparticles. The dissolution of Pt wire suggested the generation of nanoparticles was a chemical process rather than a physical process. Also, no paper supported the hypothesis that hydrogen could combust at the nanoscale in liquid media. Besides, nanoparticles were also formed during the formation of Cl_2 instead of O_2 and in acid or at a low potential, no particles generated when the bubble was formed. All these results prove the inappropriate explosion theory.

Our future work would focus on the in-situ TEM of the Pt nanoparticles generation and the comparison of nanoparticle structure between a different pH of electrolyte and different metal and alloy.

Reference

1. Zou C, Zhao Q, Zhang G, Xiong B. Energy revolution: From a fossil energy era to a new energy era. Natural Gas Industry B [Internet]. 2016;3(1):1–11. Available from: http://dx.doi.org/10.1016/j.ngib.2016.02.001

2. Rankoana SA. Human perception of climate change. Weather. 2018;73(11):367–70.

3. Gielen D, Boshell F, Saygin D, Bazilian MD, Wagner N, Gorini R. The role of renewable energy in the global energy transformation. Energy Strategy Reviews [Internet]. 2019;24(January):38–50. Available from: https://doi.org/10.1016/j.esr.2019.01.006

4. Schleussner CF, Rogelj J, Schaeffer M, Lissner T, Licker R, Fischer EM, et al. Science and policy characteristics of the Paris Agreement temperature goal. Nature Climate Change [Internet]. 2016;6(9):827–35. Available from: http://dx.doi.org/10.1038/nclimate3096

5. Obama B. The irreversible momentum of clean energy. Science. 2017;355(6321):126–9.

6. Badwal SPS, Giddey SS, Munnings C, Bhatt AI, Hollenkamp AF. Emerging electrochemical energy conversion and storage technologies. Frontiers in Chemistry. 2014;2(SEP):1–28.

7. Staffell I, Scamman D, Velazquez Abad A, Balcombe P, Dodds PE, Ekins P, et al. The role of hydrogen and fuel cells in the global energy system. Energy and Environmental Science. 2019;12(2):463–91.

8. Tesfaye M. Understanding the impact of confinement on ionomer thin film transport properties. Physiology and Behavior. 2008;95(1–2):108–13.

9. EG&G Technical Services IncU. Fuel cell handbook. Vol. 26, Phytochemistry. 1987. 1235–1236.

10. Schœnbein CF. X. On the voltaic polarization of certain solid and fluid substances . The London, Edinburgh, and Dublin Philosophical Magazine and Journal of Science. 1839;14(85):43–5.

11. Page KA, Rowe BW. An overview of polymer electrolyte membranes for fuel cell applications. ACS Symposium Series. 2012;1096:147–64.

12. Shang R, Zheng Y, Shi W, Wang X, Zhang Y. Fresh look and understanding on carnot cycle. Energy Procedia [Internet]. 2014;61:2898–901. Available from: http://dx.doi.org/10.1016/j.egypro.2014.12.213

13. Peighambardoust SJ, Rowshanzamir S, Amjadi M. Review of the proton exchange membranes for fuel cell applications [Internet]. Vol. 35, International Journal of Hydrogen Energy. Elsevier Ltd; 2010. 9349–9384. Available from: http://dx.doi.org/10.1016/j.ijhydene.2010.05.017

14. Stamenkovic VR, Strmcnik D, Lopes PP, Markovic NM. Energy and fuels from electrochemical interfaces. Nature Materials. 2016;16(1):57–69.

15. Masuda T, Sonsudin F, Singh PR, Naohara H, Uosaki K. Potential-dependent adsorption and desorption of perfluorosulfonated ionomer on a platinum electrode surface probed by electrochemical quartz crystal microbalance and atomic force microscopy. Journal of Physical Chemistry C. 2013;117(30):15704–9.

16. Kodama K, Motobayashi K, Shinohara A, Hasegawa N, Kudo K, Jinnouchi R, et al. Effect of the Side-Chain Structure of Perfluoro-Sulfonic Acid Ionomers on the Oxygen Reduction Reaction on the Surface of Pt. ACS Catalysis. 2018;8(1):694–700.

17. Wu J, Yuan XZ, Martin JJ, Wang H, Zhang J, Shen J, et al. A review of PEM fuel cell durability: Degradation mechanisms and mitigation strategies. Journal of Power Sources. 2008;184(1):104–19.

18. Yoshida T, Kojima K. Toyota MIRAI fuel cell vehicle and progress toward a future hydrogen society. Electrochemical Society Interface. 2015;24(2):45–9.

19. Jeyaraj M, Gurunathan S, Qasim M, Kang MH, Kim JH. A comprehensive review on the synthesis, characterization, and biomedical application of platinum nanoparticles. Nanomaterials. 2019;9(12).

20. Goeke RS, Datye AK, Atanassov P, St-Pierre J. Model Electrode Structures for Studies of Electrocatalyst Degradation. 2010;(January):361–8.

21. UCKO DA. Standard reduction potentials. In: Transparency Masters for Basics for Chemistry [Internet]. 1982 [cited 2020 Apr 22]. p. 38. Available from: https://www.av8n.com/physics/redpot.htm

22. Fichtner J, Garlyyev B, Watzele S, El-Sayed HA, Schwämmlein JN, Li WJ, et al. Top-Down Synthesis of Nanostructured Platinum-Lanthanide Alloy Oxygen Reduction Reaction Catalysts: Pt x Pr/C as an Example. ACS Applied Materials and Interfaces. 2019;11(5):5129–35.

23. Kabanov BN, Astakhov II, Kiseleva IG. Formation of crystalline intermetallic compounds and solid solutions in electrochemical incorporation of metals into cathodes. Electrochim Acta. 1979;24:167–71.

24. Fichtner J, Watzele S, Garlyyev B, Kluge RM, Haimerl F, El-Sayed HA, et al. Tailoring the Oxygen Reduction Activity of Pt Nanoparticles through Surface Defects: A Simple Top-Down Approach. ACS Catalysis. 2020;10(5):3131–42.

25. Duca M, Rodriguez P, Yanson AI, Koper MTM. Selective electrocatalysis on platinum nanoparticles with preferential (100) orientation prepared by cathodic corrosion. Topics in Catalysis. 2014;57(1–4):255–64.

26. Rodriguez P, Plana D, Fermin DJ, Koper MTM. New insights into the catalytic activity of gold nanoparticles for CO oxidation in electrochemical media. Journal of Catalysis [Internet]. 2014;311:182–9. Available from: http://dx.doi.org/10.1016/j.jcat.2013.11.020

27. Kromer ML, Monzó J, Lawrence MJ, Kolodziej A, Gossage ZT, Simpson BH, et al. High-Throughput Preparation of Metal Oxide Nanocrystals by Cathodic Corrosion and Their Use as Active Photocatalysts. Langmuir. 2017;33(46):13296–302.

28. Lawrence MJ, Kolodziej A, Rodriguez P. Controllable synthesis of nanostructured metal oxide and oxyhydroxide materials via electrochemical methods. Current Opinion in Electrochemistry [Internet]. 2018;10:7–15. Available from: https://doi.org/10.1016/j.coelec.2018.03.014

29. Lawrence MJ, Celorrio V, Shi X, Wang Q, Yanson A, Adkins NJE, et al. Electrochemical Synthesis of Nanostructured Metal-Doped Titanates and Investigation of Their Activity as Oxygen Evolution Photoanodes. ACS Applied Energy Materials. 2018;1(10):5233–44.

30. Rodriguez P, Tichelaar FD, Koper MTM, Yanson AI. Cathodic corrosion as a facile and effective method to prepare clean metal alloy nanoparticles. Journal of the American Chemical Society. 2011;133(44):17626–9.

31. Chen QS, Xu ZN, Peng SY, Chen YM, Lv DM, Wang ZQ, et al. One-step electrochemical synthesis of preferentially oriented (111) Pd nanocrystals supported on graphene nanoplatelets for formic acid electrooxidation. Journal of Power Sources [Internet]. 2015;282:471–8. Available from: http://dx.doi.org/10.1016/j.jpowsour.2015.02.042

32. Hersbach TJP, Kortlever R, Lehtimäki M, Krtil P, Koper MTM. Local structure and composition of PtRh nanoparticles produced through cathodic corrosion. Physical Chemistry Chemical Physics. 2017;19(16):10301–8.

33. Hersbach TJP, McCrum IT, Anastasiadou D, Wever R, Calle-Vallejo F, Koper MTM. Alkali Metal Cation Effects in Structuring Pt, Rh, and Au Surfaces through Cathodic Corrosion. ACS Applied Materials and Interfaces. 2018;10(45):39363–79.

34. Hersbach TJP, Yanson AI, Koper MTM. Anisotropic etching of platinum electrodes at the onset of cathodic corrosion. Nature Communications. 2016 Aug 24;7.

35. Feng J, Chen D, Sediq AS, Romeijn S, Tichelaar FD, Jiskoot W, et al. Cathodic Corrosion of a Bulk Wire to Nonaggregated Functional Nanocrystals and Nanoalloys. ACS Applied Materials and Interfaces. 2018;10(11):9532–40.

36. Yanson AI, Antonov P v., Yanson YI, Koper MTM. Controlling the size of platinum nanoparticles prepared by cathodic corrosion. Electrochimica Acta [Internet]. 2013;110:796–800. Available from: http://dx.doi.org/10.1016/j.electacta.2013.03.121

37. Kuriganova AB, Vlaic CA, Ivanov S, Leontyeva D v., Bund A, Smirnova N v. Electrochemical dispersion method for the synthesis of SnO2 as anode material for lithium ion batteries. Journal of Applied Electrochemistry. 2016;46(5):527–38.

38. Doronkin DE, Kuriganova AB, Leontyev IN, Baier S, Lichtenberg H, Smirnova N v., et al. Electrochemically Synthesized Pt/Al2O3 Oxidation Catalysts. Catalysis Letters. 2016;146(2):452–63.

39. Favaro M, Valero-Vidal C, Eichhorn J, Toma FM, Ross PN, Yano J, et al. Elucidating the alkaline oxygen evolution reaction mechanism on platinum. Journal of Materials Chemistry A. 2017;5(23):11634–43.

40. Monzó J, van der Vliet DF, Yanson A, Rodriguez P. Elucidating the degradation mechanism of the cathode catalyst of PEFCs by a combination of electrochemical methods and X-ray fluorescence spectroscopy. Physical Chemistry Chemical Physics. 2016;18(32):22407–15.

41. Liu J, Huang W, Chen S, Hu S, Liu F, Li Z. Facile electrochemical dispersion of bulk Rh into hydrosols. International Journal of Electrochemical Science. 2009;4(9):1302–8.

42. Yanson AI, Antonov P v., Rodriguez P, Koper MTM. Influence of the electrolyte concentration on the size and shape of platinum nanoparticles synthesized by cathodic corrosion. Electrochimica Acta [Internet]. 2013;112:913–8. Available from: http://dx.doi.org/10.1016/j.electacta.2013.01.056

43. Yanson AI, Rodriguez P, Garcia-Araez N, Mom R v., Tichelaar FD, Koper MTM. Cathodic corrosion: A quick, clean, and versatile method for the synthesis of metallic nanoparticles. Angewandte Chemie - International Edition. 2011;50(28):6346–50.

44. Smirnova N v., Kuriganova AB, Leont'Eva D v., Leont'Ev IN, Mikheikin AS. Structural and electrocatalytic properties of Pt/C and Pt-Ni/C catalysts prepared by electrochemical dispersion. Kinetics and Catalysis. 2013;54(2):255–62.

45. Chen YX, Lavacchi A, Chen SP, di Benedetto F, Bevilacqua M, Bianchini C, et al. Electrochemical milling and faceting: Size reduction and catalytic activation of palladium nanoparticles. Angewandte Chemie - International Edition. 2012;51(34):8500–4.

46. Cloud JE, McCann K, Perera KAP, Yang Y. A simple method for producing colloidal palladium nanocrystals: Alternating voltage-induced electrochemical synthesis. Small. 2013;9(15):2532–6.

47. McCann K, Cloud JE, Yang Y. Alternating voltage-induced electrochemical synthesis of colloidal Au nanoicosahedra. Journal of Nanoparticle Research. 2013;15(11).

48. Huang W, Chen S, Zheng J, Li Z. Facile preparation of Pt hydrosols by dispersing bulk Pt with potential perturbations. Electrochemistry Communications [Internet]. 2009;11(2):469–72. Available from: http://dx.doi.org/10.1016/j.elecom.2008.12.021

49. So AH, Hvid U, Mortensen MW, Mo KA. Preparation of platinum / iridium scanning probe microscopy tips Preparation of platinum / iridium scanning probe microscopy tips. 2012;3059(1999):3059–67.

50. Leontyev I, Kuriganova A, Kudryavtsev Y, Dkhil B, Smirnova N. New life of a forgotten method: Electrochemical route toward highly efficient Pt/C catalysts for low-temperature fuel cells. Applied Catalysis A: General [Internet]. 2012;431–432:120–5. Available from: http://dx.doi.org/10.1016/j.apcata.2012.04.025

51. Chen X, Chen S, Huang W, Zheng J, Li Z. Facile preparation of Bi nanoparticles by novel cathodic dispersion of bulk bismuth electrodes. Electrochimica Acta. 2009;54(28):7370–3.

52. Fuller TF, Harb JN. Electrochemical engineering.

53. George TY, Asset T, Avid A, Atanassov P, Zenyuk I v. Kinetic Isotope Effect as a Tool To Investigate the Oxygen Reduction Reaction on Pt-based Electrocatalysts – Part I: High-loading Pt/C and Pt Extended Surface. ChemPhysChem. 2020;21(6):468–468.

54. JEOL 2800 TEM | IMRI [Internet]. [cited 2020 Apr 2]. Available from: https://www.imri.uci.edu/content/jeol-2800-tem

55. Elgrishi N, Rountree KJ, McCarthy BD, Rountree ES, Eisenhart TT, Dempsey JL. A Practical Beginner's Guide to Cyclic Voltammetry. Journal of Chemical Education. 2018;95(2):197–206.

56. Macauley N, Papadias DD, Fairweather J, Spernjak D, Langlois D, Ahluwalia R, et al. Carbon Corrosion in PEM Fuel Cells and the Development of Accelerated Stress Tests. Journal of The Electrochemical Society. 2018;165(6):F3148–60.

57. Perego A, Giuffredi G, Mazzolini P, Colombo M, Brescia R, Prato M, et al. Hierarchical TiN Nanostructured Thin Film Electrode for Highly Stable PEM Fuel Cells. ACS Applied Energy Materials. 2019 Mar 25;2(3):1911–22.

58. Varcoe JR, Atanassov P, Dekel DR, Herring AM, Hickner MA, Kohl PA, et al. Anion-exchange membranes in electrochemical energy systems. Energy and Environmental Science. 2014;7(10):3135–91.

59. Macauley N, Papadias DD, Fairweather J, Spernjak D, Langlois D, Ahluwalia R, et al. Carbon corrosion in PEM fuel cells and the development of accelerated stress tests. Journal of the Electrochemical Society. 2018;165(6):F3148–60.